Available online at www.sciencedirect.com

ScienceDirect

MATTER AND RADIATION AT EXTREMES

Matter and Radiation at Extremes 2 (2017) 9−15

www.journals.elsevier.com/matter-and-radiation-at-extremes

Research Article

Effects of mode coupling between low-mode radiation flux asymmetry and intermediate-mode ablator roughness on ignition capsule implosions

Jianfa Gu*, Zhensheng Dai, Shiyang Zou, Wenhua Ye, Wudi Zheng, Peijun Gu, Shaoping Zhu

Institute of Applied Physics and Computational Mathematics, Beijing 100088, China

Received 3 July 2016; revised 15 August 2016; accepted 17 August 2016
Available online 27 September 2016

Abstract

The low-mode shell asymmetry and high-mode hot spot mixing appear to be the main reasons for the performance degradation of the National Ignition Facility (NIF) implosion experiments. The effects of the mode coupling between low-mode P2 radiation flux asymmetry and intermediate-mode $L = 24$ capsule roughness on the implosion performance of ignition capsule are investigated by two-dimensional radiation hydrodynamic simulations. It is shown that the amplitudes of new modes generated by the mode coupling are in good agreement with the second-order mode coupling equation during the acceleration phase. The later flow field not only shows large areal density P2 asymmetry in the main fuel, but also generates large-amplitude spikes and bubbles. In the deceleration phase, the increasing mode coupling generates more new modes, and the perturbation spectrum on the hot spot boundary is mainly from the strong mode interactions rather than the initial perturbation conditions. The combination of the low-mode and high-mode perturbations breaks up the capsule shell, resulting in a significant reduction of the hot spot temperature and implosion performance.

PACS codes: 52.57.-z; 52.57.Fg; 47.20.Ma

Keywords: Mode coupling; Low-mode drive asymmetry; Intermediate-mode capsule roughness; Ignition capsule implosion

1. Introduction

In the indirect-drive inertial confinement fusion (ICF) [1−3], the laser energy is converted to the thermal X-ray in a high-Z hohlraum. The X-ray radiation flux ablates the outer ablator layers of a low-Z spherical capsule, driving the capsule implosion to compress deuterium-tritium (DT) fuel and create a central hot spot with sufficiently high temperature and areal density for ignition. A series of high-convergence cryogenic layered implosion experiments have been performed on the National Ignition Facility (NIF), and the measured neutron yields are much lower than the predictions from the numerical simulations by factors of 5−10 [4]. Extensive experimental and numerical works show that low-mode asymmetry and high-mode hot spot mixing are the major reasons for implosion performance degradation [5]. The low mode asymmetries in the hot spot and the surrounding main fuel shape are mainly caused by the low-mode radiation flux asymmetry in the hohlraum [6−8]. The laser plasma instabilities (LPI), dominated by the Stimulated Raman Scattering (SRS) during the main pulse, largely reduce the deposited laser energy of the inner cone beam into the hohlraum wall. The large back-scattered energy loss is about 15% of the incident laser energy, corresponding to about 45% of the inner cone energy [9,10]. This induces a large positive (+) P2 radiation flux asymmetry imposed on the capsule surface during the peak pulse. The hot spot mix mainly results from the ablation-front instability

* Corresponding author.
E-mail address: gu_jianfa@iapcm.ac.cn (J.F. Gu).
Peer review under responsibility of Science and Technology Information Center, China Academy of Engineering Physics.

http://dx.doi.org/10.1016/j.mre.2016.09.002

growth, and the capsule support tent could be the dominant source of high-mode perturbations [5].

During the implosion process, the long-wavelength and short-wavelength perturbations are seeded to the capsule's interior by several perturbed shocks, and then be greatly amplified by the Rayleigh-Taylor (RT) instability growth [11,12] and spherical convergence Bell-Plesset (BP) growth [13]. The low-mode asymmetries can result in significant distortions of the hot spot and capsule shell shape which have been observed in the NIF implosion experiments [4,14–17]. The large amplification of the high-mode perturbations induced from the tent defect may make a large amount of ablator material enter the hot spot. The mix will largely increase the radiation loss and cool the hot spot. The combination of long- and short-wavelength perturbations will enhance the deleterious effects, leading to the break-up of the compressed shell and more ablator material mixing into the central core. Therefore, the detailed modeling of the low-mode asymmetry and the high-mode surface roughness needs to be investigated for the ignition implosions. Limited by the available computational resources, the radiation flux asymmetries and the capsule surface roughnesses including the tent defect were individually considered in the previous two-dimensional (2D) ignition capsule implosion simulations. Only the recent 3D post-shot simulations of the NIF ignition implosions have considered the radiation flux asymmetries and capsule surface roughnesses, while included the tent defect by the surrogate perturbations. This 3D work focused on the comparison between simulations and experiments, while the effects of model coupling were not studied [5]. In this paper, we will perform the 2D ignition capsule implosion simulation with both the low-mode radiation flux asymmetry and the intermediate-mode capsule surface roughness, and the effects of the mode-coupling on the perturbation growth and implosion performance will be investigated for the first time.

The rest of this paper is organized as follows. In Section 2, the simulation model is briefly described. Section 3 presents the 2D simulated flow fields of the ignition capsule implosions. Section 4 describes the theoretical analysis and discussions. The conclusions are presented in Section 5.

2. Model description

This work used a 300 eV polystyrene (CH)-ablator point design target [2]. The outer radius of the capsule is 1110 μm, and the thicknesses of the ablator and DT ice fuel layer are 160 μm and 80 μm, respectively. The capsule interior was filled with DT gas with a density of 3×10^{-4} g/cm^3. Fig. 1 plots the radiation temperature used to drive the capsule implosions. The drive profile was taken from the highly resolved 1D multi-group transport simulations using the code RDMG [18], and has been adjusted to produce the optimal Munro shock timing [19].

In this paper, a series of 2D capsule-only simulations were performed using the radiation hydrodynamic code LARED-S. It is a multi-dimensional massively parallel Eulerian mesh based code, including multi-group diffusion radiation transport, flux-limited Spitzer thermal conduction for electrons and ions, and multi-group diffusion of alpha particle. The code has been widely used in the ICF hydrodynamic instability study [8,20,21]. The opacities used in the radiation transport calculation were obtained with the relativistic Hartree-Fock-Slater (HFS) self-consistent average atom model OPINCH [22], and contributions from free-free, free-bound, bound-bound transitions were taken into account. Tabular quotidian equations of state (QEOS) were used in our simulations [23].

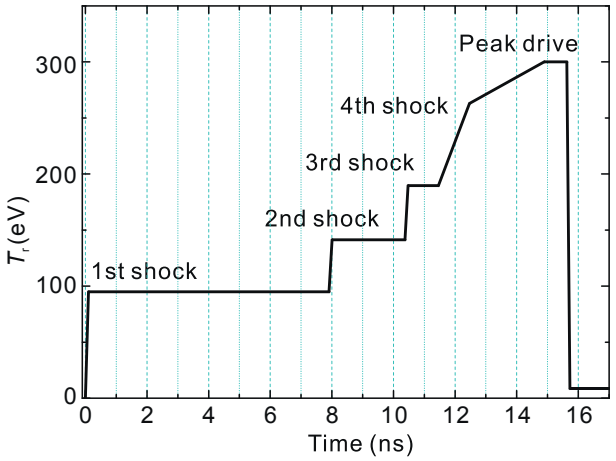

Fig. 1. The radiation temperature versus time for driving the ignition capsule implosions.

The 2D calculations used an r-θ geometry mesh. In the r direction, the simulations had 2000 cells with the maximum spatial resolution of 0.05 μm to resolve high-mode hydrodynamic instability evolution. Meanwhile, the radial meshes moved with the compressed shell to keep high resolution for the ablation front, the ablator-fuel interface, and the inner shell surface. Angularly, the 2D simulations had 240 cells from $\theta = 0$–$\pi/2$ to resolve higher modes generated by the mode-coupling effects. The simulations described here required over six months on 240 CPUs to be completed.

Before carrying out the 2D implosion simulations, we have performed highly-resolved 1D full multi-group radiation transport simulations. The highly-resolved 1D simulation results (including the ablation pressure and the position of the ablation front etc.) were used to tune the radiation drive profile of the 1D few-group diffusion simulations. The tuning made the hydrodynamic behavior of the few-group radiation diffusion simulations closely match the simulations with full multi-group radiation transport calculation. Then the 2D simulations were performed using the well-tuned radiation sources and few-group diffusion calculations, which can be completed within a reasonable time.

3. The 2D simulated flow fields of the ignition capsule implosions

In this work, several 2D simulations of the ignition capsule implosions have been performed to study the effects of both the low-mode radiation asymmetry and the outer

surface roughness on capsule stability and implosion performance. Fig. 2 shows the simulated density distribution, the equatorial hot spot X-ray image, and the radial velocity distribution at stagnation time for the ignition capsule implosion with 1.35% P2 radiation flux asymmetry. Here, the amplitude of 1.35% P2 radiation flux asymmetry is the time-averaged radiation flux asymmetry P2/P0 at the outer ablation front. In this paper, the ablation front is defined as the location of e^{-1} × max density in the CH-ablator layer. Since the capsule is driven harder on the pole than on the waist, the shell material flows away laterally from the poles (higher flux region) to the waist (lower flux region). The lateral mass flow leads to a large negative (−) P2 areal density asymmetry in the capsule shell, as shown in Fig. 2 (a). The hot spot exhibits an oblate shape seen from the equatorial view. Due to the significant P2 asymmetry, at stagnation time the polar shell has expanded outward with the radial velocity $V_r > 0$; while the heavier shell on the waist still moves inward with $V_r < 0$, as shown in Fig. 2(c). The nonuniform compression is deleterious to the conversion of the implosion kinetic energy to the hot spot internal energy. As the radiation flux asymmetry increases, the final neutron yield gradually decreases; once the flux asymmetry is larger than 1.8%, the neutron yield sharply decreases below 1 MJ, corresponding to a clear ignition cliff.

When an intermediate-mode $L = 24$ with an amplitude of $a_{24} = 0.2$ μm is imposed on the outer surface of the CH-ablator layer, and the radiation flux drive is spherically symmetric, the corresponding 2D distributions of the implosion flow field at the peak compression are shown in Fig. 3. Here, the perturbation of $L = 24$ is imposed by the $\cos(24 \cdot \theta)$ azimuthal distortion on the outer ablator surface, and θ is expressed in degrees from 0 to 2π. We can see that the intermediate-mode perturbation is greatly amplified by the RT instability growth and the BP growth during the implosion process, and produces large-amplitude spikes and bubbles in the capsule core, as shown in Fig. 3(a). The high-density spikes penetrate into and cool the hot spot, greatly reducing the volume of the high-temperature hot spot (see Fig. 3(b)). At stagnation time the spikes in the capsule shell still move inward, while the low-density bubbles expand outward and make the thin regions of capsule shell become thinner, which is deleterious to the inertial confinement of the central hot DT plasmas, as shown in Fig. 3(c).

When both the low-mode radiation flux asymmetry and intermediate-mode capsule surface roughness are imposed on the capsule during the implosion, the long-wavelength perturbation imprinted from the drive asymmetry will interact with the perturbed surface, and generate new modes by the mode-coupling effects. Fig. 4 shows the simulated distributions of the implosion flow field at the peak compression. We can see that the capsule flow field exhibits large-amplitude spikes and bubbles which result from the intermediate-mode perturbation seeded on the capsule surface. Meanwhile, the areal density of the equatorial shell is larger than the polar shell ρR, indicating a (−) P2 ρR asymmetry due to the P2 radiation flux asymmetry. The narrow spikes are significantly bent by the central turbulent-like flows as shown in Fig. 4(c). This is caused by the nonlinear mode-coupling between long- and short-wavelength modes. It is worth to note that the severe lateral mass flow thins the polar shell, and the low-density bubbles in the capsule core rapidly grow and penetrate through the compressed shell during the deceleration phase. The break-up of the polar shell (see Fig. 4(a)) causes the hot DT plasmas to escape from the hot spot, and greatly reduces the stagnation pressure and the final neutron yield.

4. Theoretical analysis and discussions

During the early time of the capsule implosion, small-amplitude perturbations grow exponentially in a linear growth stage. When the perturbation amplitudes are comparable to their wavelengths, they reach the nonlinear stage, and the growths are slowed down to an asymptotic constant rates. Meanwhile, nonlinear interactions among the growing modes become important, and many new modes are generated by the mode-coupling effects. In this work, we processed the 2D implosion simulation results at different times, and obtained the amplitudes of the multi-mode spectra on capsule surfaces by using the Fourier expansion method. Fig. 5 plots the absolute mode amplitudes as functions of the perturbation modes on the CH ablation front and the DT/CH interface at different implosion stages. The time of $t = 14.0$ ns corresponds to the in-flight stage, and at $t = 15.3$ ns the

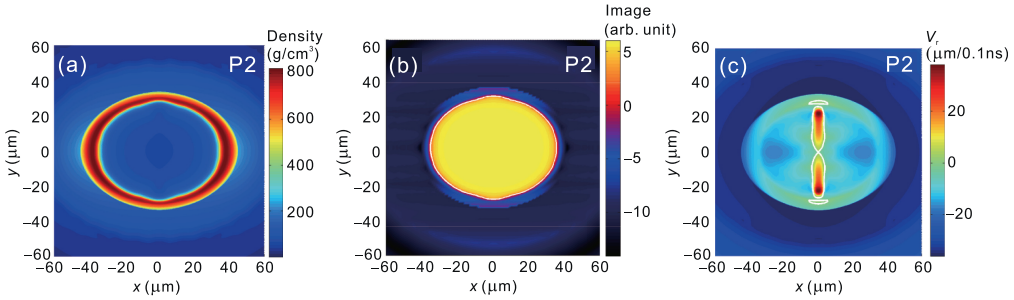

Fig. 2. (a) The density distribution, (b) post-processed X-ray self-emission images from equatorial view and (c) radial velocity V_r at stagnation time with a (+) 1.35% P2 radiation flux asymmetry applied during the ignition capsule implosion. The white lines in (b) and (c) are the 17% intensity contour of the peak X-ray emission and the contour of $V_r = 0$, respectively. The hohlraum axis is vertical at $x = 0$ μm.

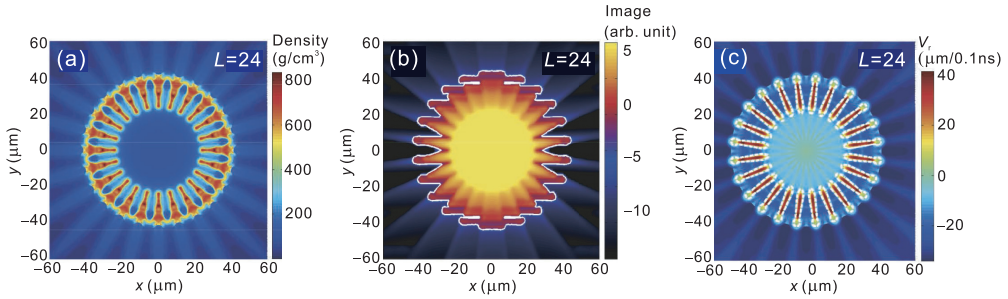

Fig. 3. (a) The density distribution, (b) post-processed X-ray self-emission images from equatorial view and (c) radial velocity V_r of the ignition capsule implosion with the $L = 24$ mode initially seeded on the outer surface of the CH-ablator layer. The amplitude of the $L = 24$ mode is 0.2 μm, and the radiation flux drive is spherically symmetric. The white lines in (b) and (c) are the 17% intensity contour of the peak X-ray emission and the contour of $V_r = 0$, respectively. The hohlraum axis is vertical at $x = 0$ μm.

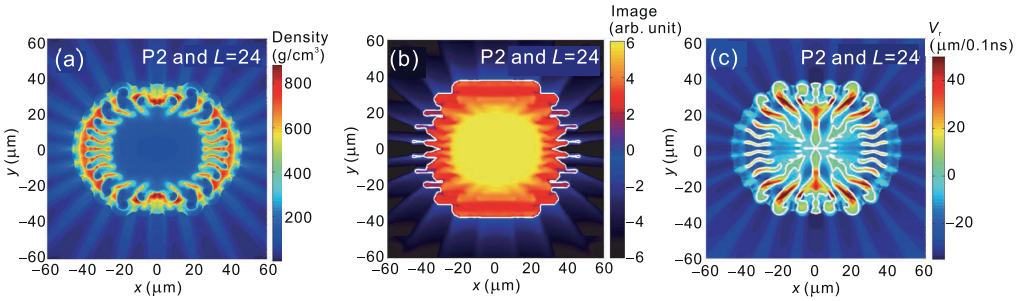

Fig. 4. (a) The 2D simulated density distribution, (b) post-processed X-ray self-emission images from equatorial view and (c) radial velocity V_r of the ignition capsule implosion with the $L = 24$ mode initially seeded on the outer surface of the CH-ablator layer. The amplitude of the $L = 24$ mode is 0.2 μm. A P2 radiation flux asymmetry with $A_2 = 1.35\%$ is imposed on the capsule surface. The white lines in (b) and (c) are the 17 % intensity contour of the peak X-ray emission and the contour of $V_r = 0$, respectively. The hohlraum axis is vertical at $x = 0$ μm.

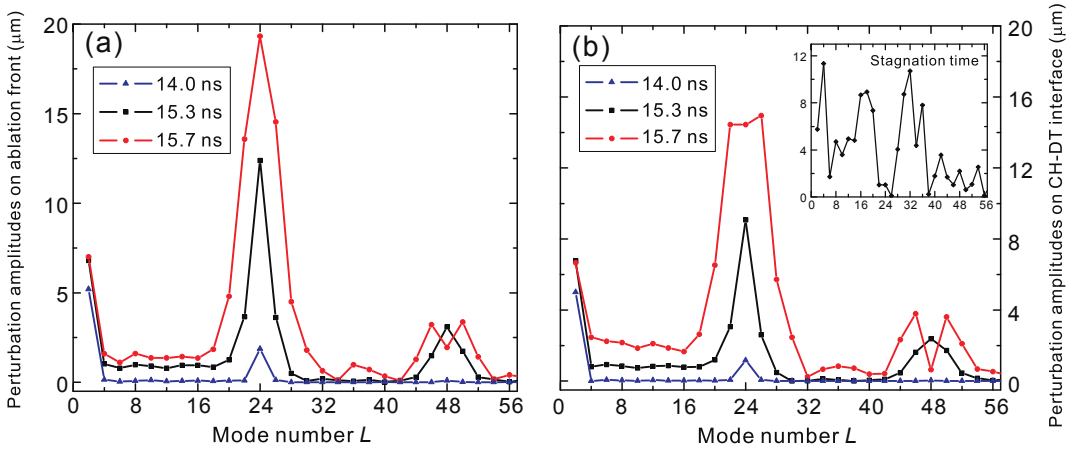

Fig. 5. (a) Amplitudes of perturbation modes L on the outer CH ablation front and (b) the CH/DT interface at different implosion stages.

strong shock reaches the capsule center. At $t = 15.7$ ns, the capsule implosion achieves the peak velocity; and $t = 15.9$ ns corresponds to the stagnation time when the capsule has the peak compression. It is shown that in the in-flight phase, the modes are in the linear growth stage, and the whole mode spectra on both the ablation front and the DT/CH interface only have two fundamental modes (including $L = 2$ imprinted from the P2 radiation flux asymmetry and $L = 24$ initially seeded on the CH ablator surface). When the strong shock wave reaches the capsule center, the perturbation growth comes in the nonlinear stage, and the mode interaction between $L = 2$ and $L = 24$ takes place. The modes of $L = 22$ and $L = 26$ are produced by $k_{24} \pm k_2$, and the position of $L = 48$ has a peak, corresponding to the second harmonic mode by $k_{24}+k_{24}$. As the implosion proceeds, the perturbation amplitudes of all the modes (including the

fundamental modes $L = 2$ and $L = 24$, second- and third-order modes) significantly increase. At the time of the peak velocity, the absolute amplitudes of the second harmonics are comparable to or larger than the value of the fundamental mode $L = 24$ on the DT/CH interface. At stagnation time, the mode spectrum is greatly broadened by the nonlinear mode-coupling effects, and the shape perturbation amplitudes of the DT/CH interface are completely different to the shape of the initial perturbation, as shown in the inset of Fig. 5(b).

By the same analyzing method, the multi-mode spectra of the main DT fuel ρR and the hot spot boundary are plotted in Fig. 6. Here, the hot spot boundary is defined as the contour of 1 keV ion temperature. It is shown that the capsule shell exhibits many new generated modes during the deceleration phase; while the amplitude of the fundamental mode $L = 24$ is greatly depressed (see the blue line in Fig. 6(a)). At stagnation time the flow fields enter the strongly nonlinear stage, and the shape perturbation amplitudes of the hot core is also completely different to the shape of the initial perturbation.

Neglecting the third-order terms, the perturbation amplitudes of the modes generated by the model-coupling approximatively satisfy the second-order mode-coupling equations [24,25]:

$$\eta_{k_i \pm k_j} \approx \mp \frac{1}{2}(k_i \pm k_j)\eta_{k_i}\eta_{k_j}, \tag{1}$$

where $k_L = 2\pi/\lambda = (L+1)/R$ denotes the mode wave number, η_{k_L} is the linear growth amplitude of mode L, and its value satisfies $\eta_{k_L} = \eta_0 \exp(a_L t)$, $L = i, j$. Here, a_L denotes the linear growth rate of mode L. According to Eq. (1), the growth rate of the second-order mode is close to $a_i + a_j$. Fig. 7 shows the temporal evolution of the amplitudes of both the fundamental modes and the generated modes. During the in-flight phase, fundamental modes $L = 2$ and $L = 24$ grow exponentially with their own linear growth rates a_2 and a_{24}, respectively; the linear growth rate of intermediate-mode $L = 24$ is obviously larger than that of low-mode $L = 2$. The modes of $L = 22$ and $L = 26$ grow exponentially with a growth rate close to $a_2 + a_{24}$, consistent with Eq. (1). However, during the late implosion stages when the amplitudes of the fundamental mode are close to their saturation amplitudes 0.1λ (implied by the dashed line in Fig. 7), the growth of the fundamental modes slows down, and the evolutions of the generated modes do not satisfy the second-order mode-coupling equation. The growth behavior is complicated by the highly nonlinear mode interactions, and needs to be investigated further.

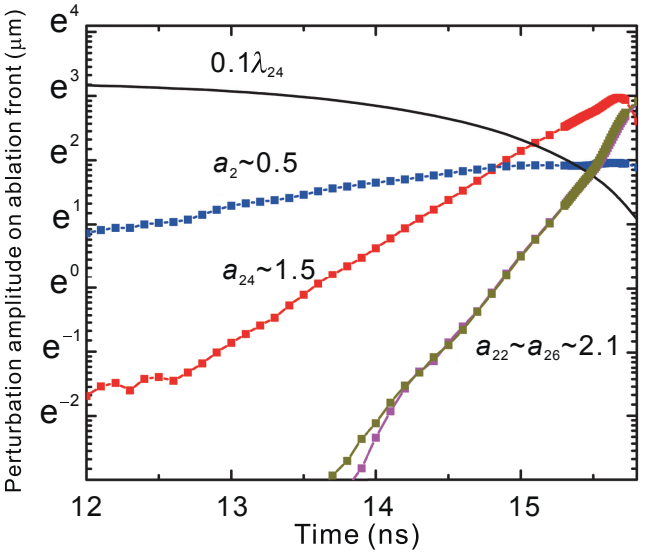

Fig. 7. Temporal evolution of the absolute amplitudes of the fundamental modes ($L = 2$ and 24) and the second-order modes ($L = 22$ and 26) on the outer ablation front. The solid line corresponds to the single mode saturation amplitude 0.1λ for $L = 24$. The values of the a_L are the slopes of the lines, which are equal to the linear growth rate of these modes.

For the absolute amplitudes of generated modes $L = 22$ and $L = 26$, Fig. 8 directly compares the 2D simulated results and the theoretical second-order mode-coupling equation (see Eq. (1)). We can see that when the simulated amplitude of fundamental mode $L = 24$ is lower than its saturation amplitude, the simulated amplitudes of the new

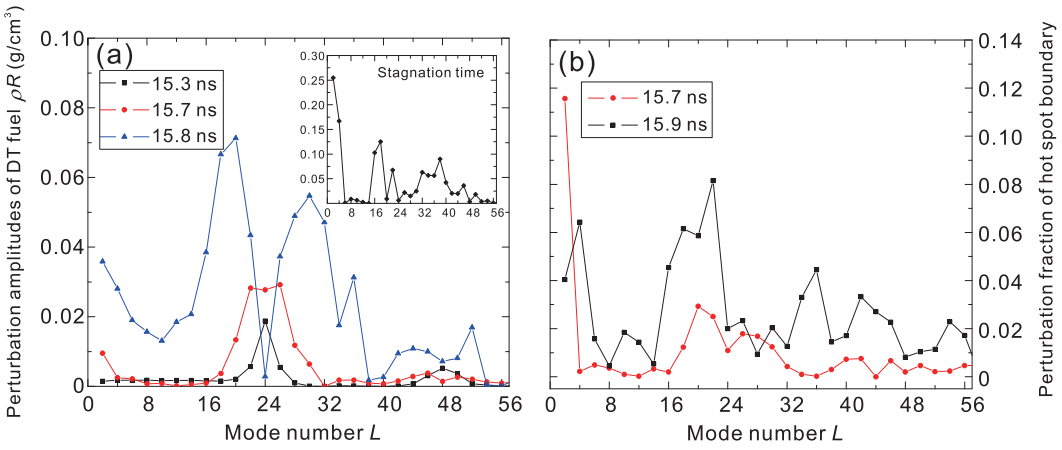

Fig. 6. (a) Amplitudes of perturbation modes L for the DT fuel areal density and (b) the hot spot boundary at different implosion stages.

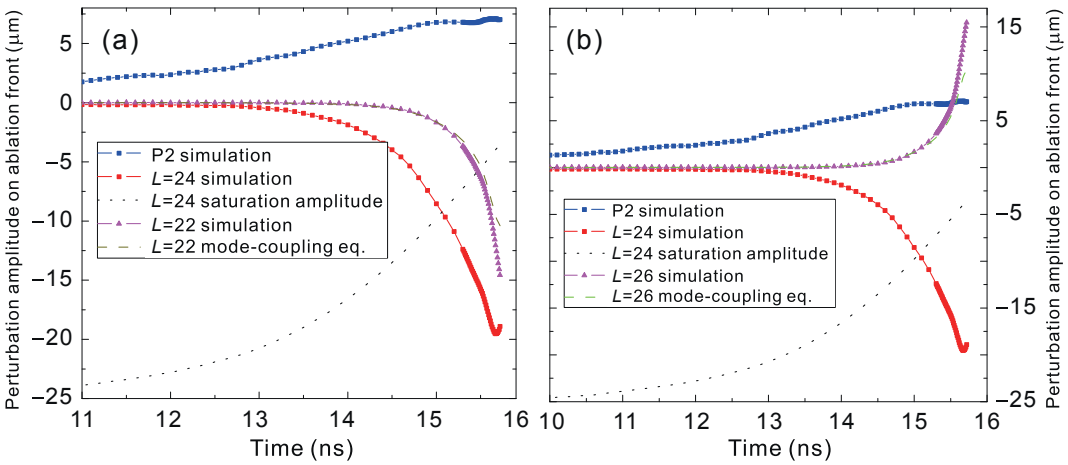

Fig. 8. Temporal evolution of the absolute amplitudes of the fundamental modes ($L = 2$ and 24) and the second-order modes (a) $L = 22$ and (b) $L = 26$ on the outer CH ablation front. The dotted lines correspond to the single mode saturation amplitude 0.1λ for $L = 24$. The dash-dot lines are obtained by post-processing 2D implosion simulation, and the dashed lines are given by the theoretical second-order mode-coupling equation.

modes generated by mode-coupling are in good agreement with the theoretical equation. However, after the amplitude of mode $L = 24$ becomes larger than its saturation amplitude, the 2D simulation values gradually deviate from the theoretical results, indicating the highly nonlinear mode-coupling effects which occur during the deceleration phase of the implosion.

Fig. 9 plots the root-mean-square (RMS) sum over the modes for the DT main fuel ρR, including the low-mode component and the relatively high-mode component. It is seen that during the early stage, the RMS of the fuel ρR is dominated by the short-wavelength modes due to their higher linear growth rates. The fundamental mode $L = 24$ plays a primary role during the acceleration phase, as shown in Fig. 9(b). However, the high modes arrive at their saturation amplitudes earlier than the low-mode perturbations, and their growths begin to slow down, while the long-wavelength modes are still in their linear stage. Therefore the fraction of the low-mode RMS sharply increases during the deceleration phase, and the long-wavelength perturbations either originated from the initial condition or generated by mode-coupling dominate the capsule distortion, as shown in Fig. 9(a).

Fig. 10 plots the minimum of angular areal density in the DT fuel versus the averaged ion temperature of the hot spot during the implosion process. Considering the mode-coupling case, the hot spot temperature and the minimum of DT fuel ρR are obviously lower than the cases without mode-coupling effects. The long-wavelength perturbations cause severe lateral mass flows, and make some regions of the compressed shell much thinner than other regions. Meanwhile, the large-amplitude bubbles grow and penetrate through the thinner shell. The combination of the low-mode and high-mode perturbations breaks up the capsule shell and allows the hot DT plasmas to escape from the hot spot, resulting in a much lower stagnation pressure and neutron yield. Besides, the strong mode interactions greatly broaden the mode spectrum and make the implosion flow turbulent, which are deleterious to the conversion from the implosion kinetic energy into the hot spot internal energy.

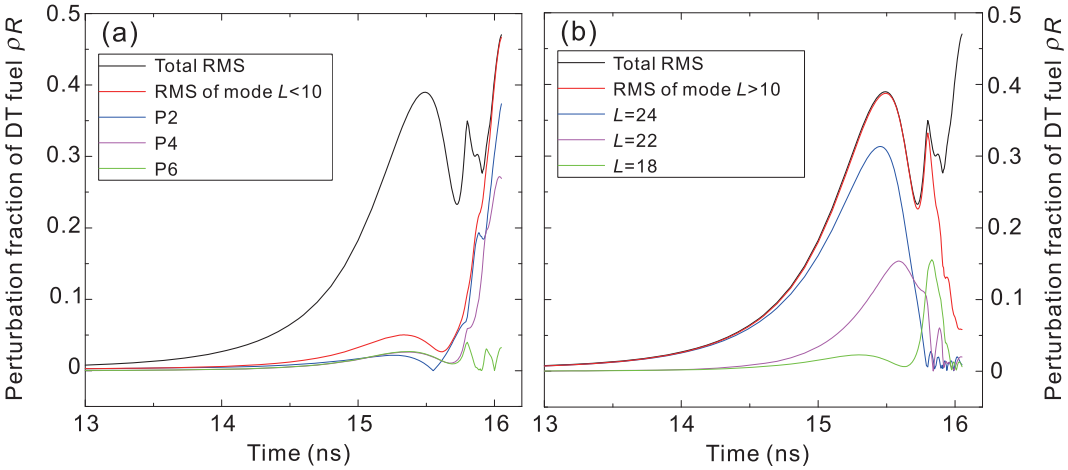

Fig. 9. Temporal evolution of the absolute RMS amplitudes of (a) low modes with $L < 10$ and (b) intermediate modes with $L \geq 10$ for the DT main fuel areal density. The black solid line is the total RMS of the fuel ρR perturbations.

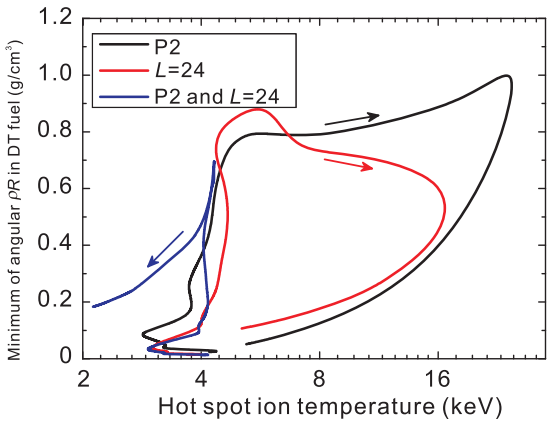

Fig. 10. The minimum of angular areal density in the DT fuel versus the averaged ion temperature of the hot spot. The arrows correspond to the direction of the temporal evolution of the implosion.

5. Conclusion

This paper has studied the effects of the nonlinear mode coupling between the low-mode perturbation imprinted from the radiation flux asymmetry and intermediate-mode capsule roughness on the implosion performance of ignition capsule. The two-dimensional implosion simulations show that the simulated amplitudes of the second-order modes generated by mode coupling are in good agreement with the second-order mode coupling equation during the acceleration phase. The implosion flow field at stagnation time not only shows large areal density P2 asymmetry in the main fuel, but also generates large-amplitude spikes and bubbles. In the deceleration phase, the increasing mode coupling generates more new modes, and the distorted flow field is dominated by the long-wavelength perturbations. The combination of the low-mode and high-mode perturbations breaks up the capsule shell, and greatly reduces the hot spot temperature and the minimum of angular areal density in the DT fuel shell. It should be mentioned that the ICF implosions involve many other complex physics processes such as 3D flow effects, capsule support tent, etc, and this work only considered two modes rather than the whole perturbation spectra. So further works are required to research the effects of the mode-coupling among the multi-mode spectra on the ignition capsule implosion performance.

Acknowledgments

This work is supported by the National Natural Science Foundation of China under Grant Nos. 11575034, 11275031, 11401033, and 91330205.

References

[1] S. Atzeni, J. Meyer-ter-Vehn, The Physics of Ineritial Fusion, Oxford Science, Oxford, 2004.
[2] J.D. Lindl, Development of the indirect-drive approach to inertial confinement fusion and the target physics basis for ignition and gain, Phys. Plasmas 2 (1995) 3933.
[3] J.D. Lindl, P. Amendt, R.L. Berger, S.G. Glendinning, S.H. Glenzer, et al., The physics basis for ignition using indirect-drive targets on the National ignition Facility, Phys. Plasmas 11 (2004) 339.
[4] M.J. Edwards, P.K. Patel, J.D. Lindl, L.J. Atherton, S.H. Glenzer, et al., Progress towards ignition on the National Ignition Facility, Phys. Plasmas 20 (2013) 070501.
[5] D.S. Clark, C.R. Weber, J.L. Milovich, J.D. Salmonson, A.L. Kritcher, et al., Three-dimensional simulations for low foot and high foot implosion experiments on the National Ignition Facility, Phys. Plasmas 23 (2016) 056302.
[6] R.P.J. Town, D.K. Bradley, A. Kritcher, O.S. Jones, J.R. Rygg, et al., Dynamic symmetry of indirectly driven inertial confinement fusion capsules on the National Ignition Facility, Phys. Plasmas 21 (2014) 056313.
[7] A.L. Kritcher, R.P.J. Town, D.K. Bradley, D.S. Clark, B.K. Spears, et al., Metrics for long wavelength asymmetries in inertial confinement fusion implosions on the National Ignition Facility, Phys. Plasmas 21 (2014) 042708.
[8] J.F. Gu, Z.S. Dai, Z.F. Fan, S.Y. Zou, W.H. Ye, et al., A new metric of the low-mode asymmetry for ignition target designs, Phys. Plasmas 21 (2014) 012704.
[9] J.L. Kline, D.A. Callahan, S.H. Glenzer, N.B. Meezan, J.D. Moody, et al., Hohlraum energetics scaling to 520 TW on the National Ignition Facility, Phys. Plasmas 20 (2013) 056314.
[10] J.D. Moody, D.A. Callahan, D.E. Hinkel, P.A. Amendt, K.L. Baker, et al., Progress in hohlraum physics for the National Ignition Facility, Phys. Plasmas 21 (2014) 056317.
[11] L. Rayleigh, Scientific Papers, II, Cambridge University Press, Cambridge, England, 1900, p. 200.
[12] G. Taylor, The instability of liquid surfaces when accelerated in a direction perpendicular to their planes, Proc. R. Soc. Lond. 201 (1950) 192.
[13] M.S. Plesset, On the stability of fluid flows with spherical symmetry, J. Appl. Phys. 25 (1954) 96.
[14] J.D. Lindl, Overview and Status of the National Ignition Campaign on the NIF, Presentation to Ignition Science Workshop, 2012.
[15] C. Cerjan, P. Springer, S.M. Sepke, Integrated diagnostic analysis of inertial confinement fusion capsule performance, Phys. Plasmas 20 (2013) 056319.
[16] A.B. Zylstra, J.A. Frenje, F.H. Séguin, J.R. Rygg, A. Kritcher, et al., In-flight observations of low-mode ρR asymmetries in NIF implosions, Phys. Plasmas 22 (2015) 056301.
[17] N.B. Meezan, L.F. Berzak Hopkins, S. Le Pape, L. Divol, A.J. MacKinnon, et al., Cryogenic tritium-hydrogen-deuterium and deuterium-tritium layer implosions with high density carbon ablators in near-vacuum hohlraums, Phys. Plasmas 22 (2015) 062703.
[18] G.T. Feng, K. Lan, D.X. Lai, A comparison between two averaging methods of multi-group parameters in ICF radiation transfer calculation, Chin, J. Comput. Phys. 18 (2001) 3.
[19] D.H. Munro, P.M. Celliers, G.W. Collins, D.M. Gold, L.B. Da Silva, et al., Shock timing technique for the National Ignition Facility, Phys. Plasmas 8 (2001) 2245.
[20] W.H. Ye, W.Y. Zhang, X.T. He, Stabilization of ablative Rayleigh-Taylor instability due to change of the Atwood number, Phys. Rev. E 65 (2002) 057401.
[21] J.F. Gu, Z.S. Dai, S.Y. Zou, P. Song, W.H. Ye, et al., New tuning method of the low-mode asymmetry for ignition capsule implosions, Phys. Plasmas 22 (2015) 122704.
[22] F.J.D. Serduke, E. Minguez, S.J. Davidson, C.A. Iglesias, WorkOp-IV summary: Lessons from iron opacities, J. Quant. Spectrosc. Radiat. Transf. 65 (2000) 527.
[23] R.D. More, K.H. Warren, D.A. Young, G.B. Zimmerman, A new quotidian equation of state (QEOS) for hot dense matter, Phys. Fluids. 31 (1988) 3059.
[24] D. Ofer, D. Shvarts, Z. Zinamon, S.A. Orszag, Mode coupling in nonlinear Rayleigh-Taylor instability, Phys. Fluids B 4 (1992) 3549.
[25] D. Ofer, U. Alon, D. Shvarts, R.L. McCronry, C.P. Verdon, Mode coupling for the nonlinear multimode Rayleigh-Taylor instability, Phys. Plasmas 3 (1996) 3073.